Topics in Catalysis (2023) 66:750–760
https://doi.org/10.1007/s11244-022-01737-9

ORIGINAL PAPER

Pd-Doped SSZ-13 for Low-T NOx Adsorption: an Operando FT-IR Spectroscopy Study

Y. Hamid[1] · R. Matarrese[1] · S. Morandi[2] · L. Castoldi[1] · L. Lietti[1]

Accepted: 24 October 2022 / Published online: 17 November 2022

Abstract

In this study, mechanistic aspects of NO adsorption/desorption over a home-made Pd/SSZ-13 passive NOx adsorber (PNA) catalyst are investigated. Operando FT-IR spectroscopy and microreactor experiments are performed to envisage the performance of the catalyst and the pathway involved in NO adsorption, with particular emphasis to the impact of species such as C_3H_6 and CO. In the absence of C_3H_6 and CO, NO is observed to adsorb as nitrosyls (anhydrous and hydrated) over both Pd^{2+} and Pd^{+} species, and as nitrates. 80 $\mu molNO_x/g_{cat}$ (NO/Pd molar ratio of 0.8) are adsorbed. The stability of nitrosyls is higher in comparison to the nitrates in that the former initially dehydrate and further decompose at elevated temperatures (> 300 °C) leading to the evolution of NO. The presence of CO and C_3H_6 negatively affects the amounts of NO adsorbed (53 and 45 $\mu molNO_x/g_{cat}$, respectively) due to the reduction of Pd sites. CO admission to the catalyst forms a variety of carbonyl species over Pd^{2+}, Pd^{+} and Pd^{0} sites which upon NO admission are readily displaced and NO is adsorbed as hydrated/anhydrous nitrosyls of Pd^{n+}. The nitrosyls so formed exhibit lower thermal stability in comparison to nitrosyls observed in the absence of CO and decompose below 300 °C. The addition of C_3H_6 leads to the apparent formation of oxidized species like acetone, acrolein and acetates, besides propylene adsorption. The NO adsorption in the presence of C_3H_6 leads to the formation of $Pd^{n+}(NO)(X)$ complexes; upon heating the decomposition of this complexes is observed at low temperatures along with propylene and water desorption. Formation of organic nitro-compounds is also observed that decompose at higher temperatures.

Keywords Pd-doped zeolites · Cold-start · NOx adsorbers · PNA · Pd · SSZ-13

1 Introduction

The mobile transportation is an indispensable part of modern life. However, despite its many positive aspects, it is closely associated with the hazards to the environment and human health. In an attempt to counter the increasing transport volume, and the associated risk of harm to air quality, stringent regulations on vehicle emissions are being implemented around the world. Mitigating emissions of hydrocarbons (HCs), carbon monoxide (CO), nitrogen oxides (NO_x), and particulate matter (PM) from gasoline and diesel engines are essential to meet current and future legislation standards. For diesel engines, and in general lean-burn engines, CO is controlled by a diesel oxidation catalyst, PM by a diesel particulate filter, while NO_x are controlled by a selective catalytic reduction (SCR) or a NO_x-storage reduction (NSR) catalyst. Nevertheless, the stated NO_x control technologies cannot operate properly below 200 °C, and therefore during cold start period significant amount of NO_x are released into the atmosphere without any catalytic treatment [1–3]. Consequently, under Tier 3 regulations of the US Environmental Protection Agency, automobiles must employ additional steps to curtail the amount of NOx and HC emitted during cold-start period [4].

A possible solution is the adoption of low temperature NO_x adsorbers, the so-called passive NOx adsorbers (PNAs) that have been proposed to specifically address the low temperature emission of NO_x [1–9, 5–8]. The PNAs are placed upstream the $DeNO_x$ devices and are able to temporarily

✉ L. Lietti
luca.lietti@polimi.it

[1] Laboratory of Catalysis and Catalytic Processes, Dipartimento di Energia, Politecnico di Milano, Via La Masa 34, Milan, Italy

[2] Dipartimento di Chimica, NIS Center and INSTM Reference Center, Università di Torino, Via P. Giuria 7, 10125 Turin, Italy

store NO_x at low temperature (< 150 °C). The stored NO_x are released at higher temperature, thereby enabling their downstream reduction [2, 7, 10]. A typical PNA formulation is based on a metal dispersed over a high surface area support, such as a zeolite. In particular, Pd exchanged zeolite systems are predominantly attractive due to their higher trapping efficiency, storage capacity, hydrothermal stability and resistance to sulphur and hydrocarbon poisoning [1, 3–6, 11–15]. However, the performances of these systems should be optimized in view of the high cost of the active Pd component, and therefore it is important to fully understand the behavior of such systems. This has motivated our work where an investigation has been carried out by means of operando FT-IR spectroscopy to deepen mechanistic aspects related to the low-T adsorption/desorption of NO_x and to envisage the performance of catalyst under the impact of species present in the exhaust gases like CO and propylene. To this end, a small-pore size zeolite (chabazite) doped with Pd has been considered, and the impact of such species on the NO_x trapping and desorption characteristics of the Pd-promoted zeolite has been evaluated.

2 Materials and Methods

2.1 Catalyst Preparation and Characterization

The Pd-doped chabazite used in this study (Pd_1/SSZ-13, Pd loading 1% w/w) has been prepared starting from a commercial zeolite (ACS Chemical, Si/Al = 10–15), available in its H-form. The Pd_1/SSZ sample was prepared by impregnation of the zeolite support in excess of solvent using aqueous $Pd(NO_3)_2$ (solution at 4.5% Pd, Sigma-Aldrich), followed by drying in air at 80 °C overnight [16]. The dried precursor has been calcined with a two-ramp heating program, from room temperature up to 500 °C (rate: 1 °C/min, hold at 500 °C 3 h) and then from 500 °C up to 750 °C (rate 5 °C/min, hold at 750 °C 2 h).

The prepared catalyst has been fully characterized by different techniques including in-situ FT-IR characterization by CO and NO adsorption, XRD and HRTEM. As reported elsewhere [manuscript in writing by Matarrese et al.], Pd is present on such sample as isolated Pd^+ and Pd^{2+} formed by ion exchange on the Brønsted acid sites of the zeolite, and as Pd^+ and Pd^{2+} species belonging to PdO_x clusters and particles on the external surface of the zeolite.

2.2 Reactivity Studies

Standard NO_x adsorption experiments were conducted both in a microreactor apparatus and in an operando FT-IR cell. In the first case, 100 mg of powdered catalysts, sieved at 70–100 μm, were loaded in a quartz microreactor with an internal diameter of 8 mm. The outlet of the reactor is directly connected to a mass spectrometer (ThermoStar 200, Pfeiffer Vacuum), a UV-analyzer specific for NO, NO_2, NH_3 (Limas 11HW, ABB), and a micro gas-chromatograph (3000A, Agilent) for gas on-line analysis. The adopted protocol for the NO adsorption/desorption tests (standard test) consisted in an initial pretreatment under a flow of O_2 (3% v/v) and H_2O (2.5% v/v) (balance He) at 500 °C for 30 min (flow rate 100 Ncm^3/min). Then the catalyst was cooled down to 80 °C and stabilized at this temperature for 30 min (phase 1). At this temperature 300 ppm of NO are stepwise added to the gas mixture for 75 min (phase 2). Then, NO supply is closed, and the catalyst is heated under temperature programming (TPD) up to 500 °C (heating rate 10 °C/min) (phase 3). O_2 (3% v/v) and H_2O (2.5% v/v) were always flowing during the whole experiment.

The amounts of NO_x stored during the experiments can be obtained both from phase 2 (as difference between the inlet and outlet NO concentration) or phase 3, estimating the amounts of desorbed NO_x. In a typical experiment, these 2 values differ less than 5–10%.

The effect of the presence of CO and C_3H_6 on the NO adsorption/desorption characteristics has also been investigated. In this case 300 ppm of CO or 400 ppm of C_3H_6 have been fed to the reactor at 80 °C during phase 1, i.e., before NO adsorption. Then phases 2 (NO adsorption) and 3 TPD have been carried out while keeping CO or C_3H_6, along with O_2 and H_2O. In the case of CO, the effect of the addition of CO after NO adsorption has also been investigated. Accordingly, in this case CO (800 ppm) has been added during NO adsorption (phase 2), and eventually phase 3 (TPD) has been carried out.

The same experimental procedure and protocol adopted for microreactor experiments has been used in the operando FT-IR reactor cell as well. In this case the catalyst has been formed in self-supported wafers (7–12 mg cm^{-2}) and loaded in the IR cell reactor (#CSX, AABSPEC). Due to the small catalyst loading, the operando reactor has been operated at a higher space velocity was higher due to technical limitations in the minimum flow rate fed to the cell (25 Ncm^3/min). The IR spectra (reported as difference spectra, using as background the spectrum obtained after the pre-treatment) were collected with a FT-IR Vertex 70 (Bruker, Billerica, MA, USA) spectrometer with 4 cm^{-1} spectral resolution. The outlet of the IR cell is diluted with N_2 and connected to a FT-IR Multigas 2030 (MKS) for gas analysis.

3 Results and Discussion

3.1 NO Adsorption/Desorption

The gas-phase concentration profiles obtained upon NO adsorption and subsequent TPD in the microreactor

(standard test) are shown in Fig. 1a. Upon addition of NO (phase 2 in Fig. 1a), the NO concentration increases with time reaching slowly the inlet concentration value (300 ppm): this indicates that the catalyst is fairly able to trap a certain amount of NO. Small amounts of NO_2 (few ppm, hardly visible in the figure) also evolve during the NO storage.

The total amount of NO_x adsorbed on Pd/CHA upon NO admission has been estimated to be near 80 μmol/g_{cat}, corresponding to a NO/Pd molar ratio of 0.8. This value suggests that the presence of Pd species as cluster and/or big particles which do not participate in the NO_x adsorption is quite low.

The nature of the adsorbed species can be identified by operando FT-IR spectroscopy. As shown in Fig. 2, the principal IR features are observed in the region 1900–1700 cm^{-1}, at about 1626 cm^{-1} and in the region 1550–1300 cm^{-1}. The bands in the 1900–1700 cm^{-1} region are related to Pd^{n+} nitrosyls; in particular it is possible to assign the band at 1856 cm^{-1} to nitrosyl species of Pd^{2+}, the band at 1810 cm^{-1} to nitrosyl species of Pd^{+} [14, 17] while the feature at 1750 cm^{-1} is likely to be associated to $Pd^{+}(NO)(H_2O)$ complex. In fact, according to the literature, the coordination of a water molecule to $Pd^{n+}NO$ is expected to decrease the

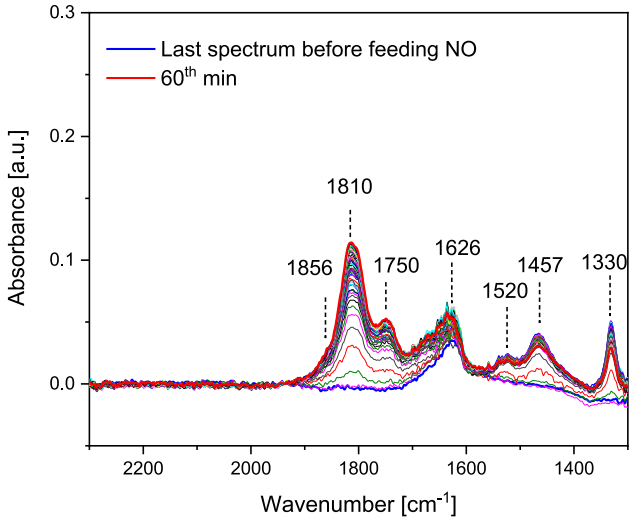

Fig. 2 Operando FT-IR spectra collected during the NO adsorption at 80 °C. Experimental conditions: storage phase (phase 2) NO (300 ppm) + O_2 (3%) + H_2O (2, 5%) in He

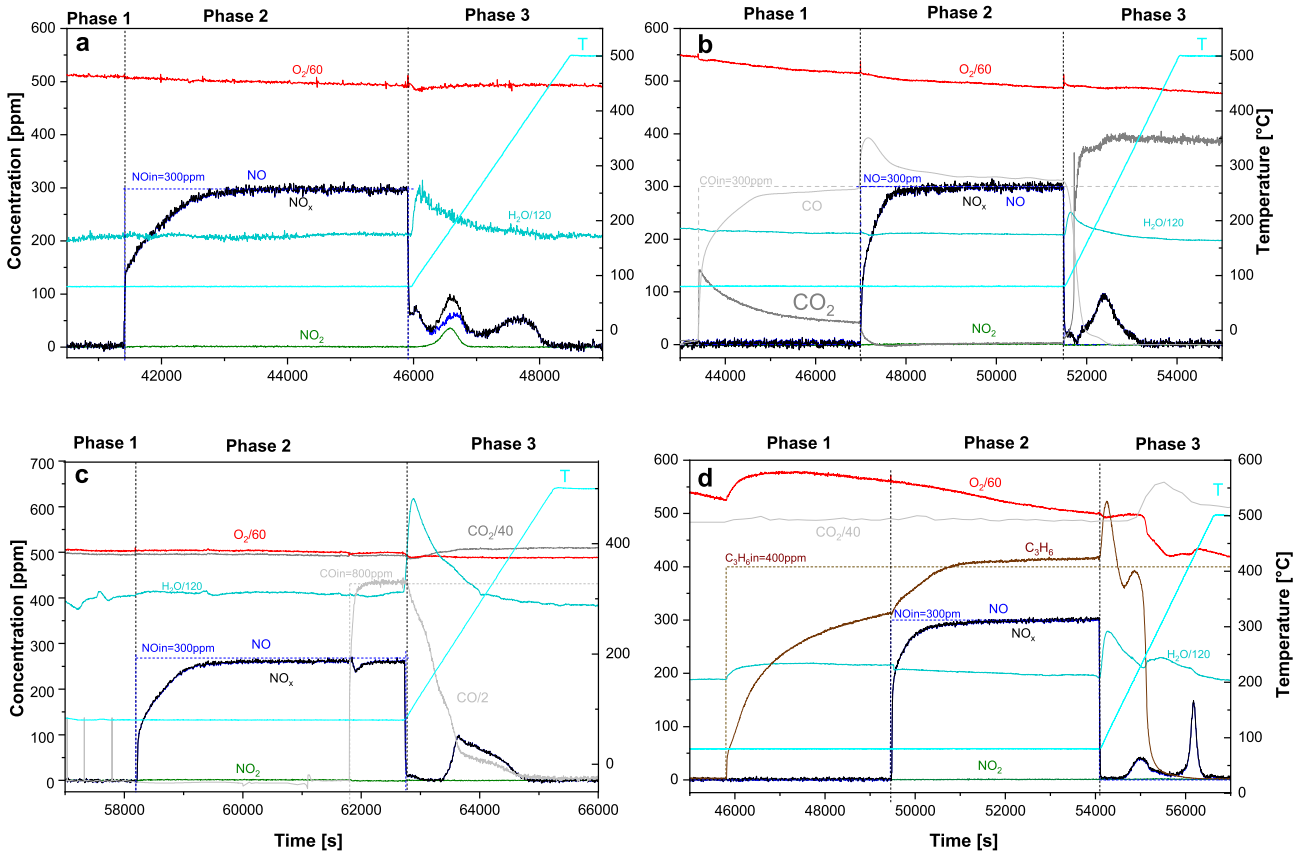

Fig. 1 NO adsorption at 80 °C (phase 2) and subsequent TPD (phase 3) experiments over Pd_1/SSZ-13 calcined at 750 °C in the presence of: (**a**) standard test, (**b**) and (**c**): effect of CO addition prior and after NO admission, respectively, (**d**) effect of C_3H_6 addition prior NO adsorption

NO stretching by ca. 50 cm^{-1} [18–21]. This means that the band present at about 1810 cm^{-1}, which appears broad and much more intense than the others, is reasonably composed by Pd^{+} nitrosyls, as suggested above, and also by $Pd^{2+}(NO)(H_2O)$ complexes. At variance, Song et al. [22] attributed the band observed around ~ 1750 cm^{-1} to hydrated $Pd^{2+}(NO)(H_2O)_x$ complex in a different constrained location, but in a FER zeolite. The picture is however rather complex in view of the fact that the Pd^{+} species may also have contributions near 1850 cm^{-1}, as recently suggested in the literature [4, 23]. Formation of such nitrosyls species occurs by direct NO adsorption on Pd sites, e.g.:

$$Pd^{2+}\left(H_2O\right) + NO \rightarrow Pd^{2+}(NO)\left(H_2O\right) \quad (1)$$

Reduction of Pd^{2+} sites to Pd^{+} sites with NO_2 evolution may also take place, as suggested in the literature [see e.g. 11, 12], although the tiny amounts of NO_2 evolved durifng NO adsorption suggests that this mechanism is not very active under our operating conditions:

$$2[PdOH]^{+} + NO \rightarrow 2Pd^{+} + NO_2 + H_2O \quad (2)$$

where $[PdOH]^{+}$ represents a Pd^{2+} species. NO is then adsorbed over Pd^{+}, leading to the following overall stoichiometry for NO adsorption:

$$2[PdOH]^{+} + 3NO \rightarrow 2Pd^{+}NO + NO_2 + H_2O \quad (3)$$

Notably, the characteristic peak at 2160 cm^{-1} corresponding to the coordinated NO^{+} species is not present in our spectra, due to the presence of water. The band at 1626 cm^{-1} is related to the bending mode of adsorbed molecular water, which is already present before feeding NO. Finally, the bands in the region 1500–1300 cm^{-1} are assigned to surface nitrates. In particular, the bands at 1457 cm^{-1} and 1330 cm^{-1} can be possibly associated to $\nu_{asym.}(NO_2)$ and $\nu_{sym.}(NO_2)$ modes of monodentate nitrates, while the band at 1520 cm^{-1} is characteristic of bidentate nitrates [24]. Nitrates formation likely involves PdO clusters and the participation of oxygen [12]:

$$PdO + 2NO + 3/2O_2 \rightarrow Pd\left(NO_3\right)_2 \quad (4)$$

The observed nitrate bands initially increase and then slightly decrease upon increasing the time on stream, as opposed to nitrosyl that monotonically increases with time.

Accordingly, both Pd^{+} and Pd^{2+} nitrosyls, anhydrous and hydrated, are formed upon NO adsorption, along with nitrates formed on PdO species.

After the NO storage phase (phase 2 of Fig. 1), the NO supply was closed, and the catalyst was heated under TPD up to 500 °C (phase 3). This allowed to analyze the thermal stability of the stored NO_x species. The gas-phase data are shown in Fig. 1, while the corresponding FT-IR spectra are reported in Fig. 3. Three different peaks are observed in the gas phase, i.e., a low-T peak just after the NO closure, a peak with maximum near 200 °C accompanied by NO_2 evolution and eventually a broad high-T peak in the range 300–400 °C.

Looking at the surface (Fig. 3), during the initial heating of the catalyst up to 200 °C (Fig. 3a), the band observed at 1750 cm^{-1} associated to hydrated $Pd^{+}(NO)(H_2O)$ complex gradually decreases and eventually disappears; the band at 1810 cm^{-1}, associated to both $Pd^{+}NO$ and $Pd^{2+}(NO)(H_2O)$ complex, also decreases. Simultaneously, the shoulder at 1856 cm^{-1} ascribed to nitrosyl species of Pd^{2+} markedly grows in intensity. These features vividly indicate the formation of anhydrous nitrosyls from the corresponding hydrated ones. This suggestion is further confirmed by the isosbestic point visible in the spectra of Fig. 3a, and by the release of water in the gas phase. In the same temperature range and in line with the surface dehydration, the band at 1626 cm^{-1}, assigned to adsorbed water, decreases. Finally, the bands related to monodentate and bidentate nitrates (in the region 1500–1300 cm^{-1}) rapidly decrease upon heating and are almost completely removed below 160 °C.

Upon further heating of the catalyst, no significant changes are visible in the 200–300 °C T-range (Fig. 3b)

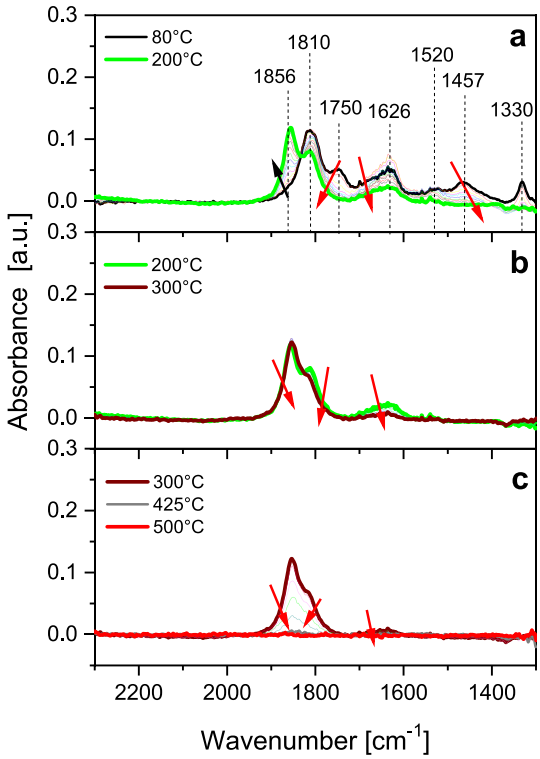

Fig. 3 FT-IR spectra collected during the TPD after NO adsorption at 80 °C (phase 3 of Fig. 1a). (**a**) 80 to 200 °C, (**b**) 200 to 300 °C, (**c**) 300 to 500 °C. Experimental conditions: TPD in O_2 (3%) + H_2O (2.5%) in He from 80 to 500 °C (10 °C/min)

whereas upon further increasing the temperature up to 500 °C (Fig. 3c) the band observed at 1626 cm^{-1} associated with adsorbed water completely disappears, while the bands related to anhydrous Pd^{+} and Pd^{2+} nitrosyls (1810 and 1856 cm^{-1}, respectively) progressively decrease and eventually disappear above 425 °C.

According to FT-IR data, the low-T NO (and NO_2) peaks observed in the TPD trace below 200 °C can be associated to nitrosyls dehydration and nitrate decomposition, that hence contribute in the low-temperature NO_x desorption peak [6]. At variance, the broad high-T NO desorption peak is related to the decomposition of nitrosyls, both of Pd^{+} and Pd^{2+}. Early studies by Khivantsev et al. [11] demonstrated the Pd^{2+} reduction by NO to form Pd^{+} nitrosyls. They also demonstrated by DFT studies that the binding of NO to Pd^{+} sites is stronger than that of Pd^{2+} sites, as also observed by Kim et al. [4]. This suggests that Pd^{+} nitrosyls are responsible for the high-temperature feature of the broad NO desorption peak while Pd^{2+} nitrosyls for the low-temperature shoulder of the NO peak. If this is the case, one may expect that that the FT-IR bands 1810 cm^{-1}, associated to nitrosyls of Pd^{+}, decreases slower than the band at 1856 cm^{-1} (Pd^{2+} nitrosyls). At variance, the two bands show an almost simultaneous decrease during the catalyst heating. This may be related to the fact that Pd^{+} nitrosyls contribute to the band at 1856 cm^{-1} as well, as indicated by some authors (Kim et al. [4]; Mandal et al. [23]). However, the role of oxygen present in the gaseous stream in the oxidation of Pd^{+} species into Pd^{2+} cannot be excluded, thus affecting the observed ratio of the intensity of the bands at 1810 and 1856 cm^{-1}, as in fact reported in ref [14].

3.2 NO Adsorption/Desorption in the Presence of CO

In this section the effect of CO presence on NO_x adsorption/desorption has been investigated. As previously reported (see experimental), in this experiment CO is adsorbed before and after NO and eventually the catalyst is heated in the presence of CO (along with water and oxygen).

When CO is admitted before NO (phase 1 in Fig. 1b), the CO concentration reaches the inlet value (300 ppm) showing a concomitant evolution of CO_2, arising from CO oxidation. The CO_2 evolution is not constant (i.e., is not a continuous oxidation process) but shows an initial peak and then decreases, being likely associated with the reduction of the Pd sites as will be discussed below.

The FT-IR spectra recorded during the same phase have been displayed in Fig. 4a; the principal peaks were observed in the regions of 2160–2080 cm^{-1}, 1970–1860 cm^{-1} and 1700–1600 cm^{-1}. The bands at 2152, 2132 and 2089 cm^{-1} have been associated to linear mono-carbonyls of Pd^{2+}, Pd^{+} and Pd^{0}, respectively [25, 26], thus indicating the reduction of the Pd sites. Of note, these bands show frequencies characteristic of Pd species belonging to particles, pointing out that isolated Pd^{n+} cations, eventually formed by ion exchange on the Brønsted acid sites of the zeolite are not accessible. Indeed, isolated Pd^{n+} cations are characterized by the formation of di-carbonyl species, which show bands at higher frequencies, e.g., in the 2200–1900 cm^{-1} range, especially for Pd^{2+} [9, 17, 21]. The bands at 1961 and 1945 cm^{-1} could be assigned to bridged carbonyls of Pd^{+}/Pd^{0} sites, while the more prominent band at 1869 cm^{-1} to the multi-bridged carbonyls on particles [28] or small clusters like Pd_3^{0} and Pd_3O [5, 28]. In any case, FT-IR data clearly

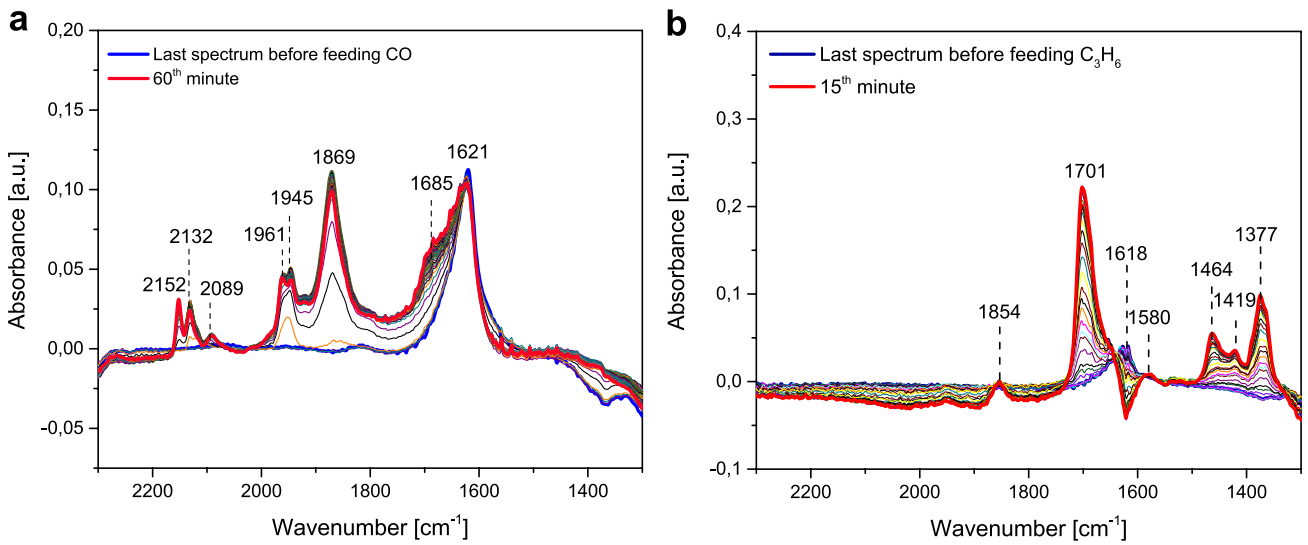

Fig. 4 FT-IR spectra collected at 80 °C upon admission of: (**a**) CO and (**b**) C_3H_6

points out presence of reduced Pd sites, formed upon reaction with CO. Adsorbed water is also observed, as pointed out by the band at 1621 cm^{-1}, while the shoulder that is apparent at 1685 cm^{-1} is still unclear.

Under CO flow, NO was admitted to the reactor at 80 °C (phase 2 of Fig. 1b). The NO concentration increases steadily reaching the inlet concentration value (300 ppm), but part of the fed NO is adsorbed on the catalyst. Roughly 53 µmol/g_{cat} of NO have been adsorbed, corresponding to a NO/Pd molar ratio of 0.5. Of note, a simultaneous release of CO is observed upon NO adsorption, pointing out that CO is displaced by NO from the same storage sites. The results of FT-IR surface analysis upon NO admission in the presence of CO are shown in Fig. 5a. In line with the CO displacement by NO, an erosion of the various bands of linear and bridged Pd carbonyls present in the region 2150–1860 cm^{-1} is observed, while new bands are formed and specifically a new single peak at 1800 cm^{-1} with a shoulder at 1755 cm^{-1}, associated to the formation of Pd nitrosyls. This indicates that NO is adsorbed as nitrosyls (hydrated/anhydrous on Pd^{n+}) at the expenses of carbonyls. Notably, a new very weak band at around 2140 cm^{-1} is also formed possibly relating to the co-adsorption of CO and NO on [Pd (II) $(OH)]^+$ as also suggested by Khivantsev et al. [14]. This species may also contribute to the band at 1800 cm^{-1}. At variance with the experiments carried out without CO, no nitrate formation has been observed.

The results of the TPD part of the experiment (phase 3) carried out in the presence of CO (Fig. 1b) shows differences with respect to the same experiment carried out

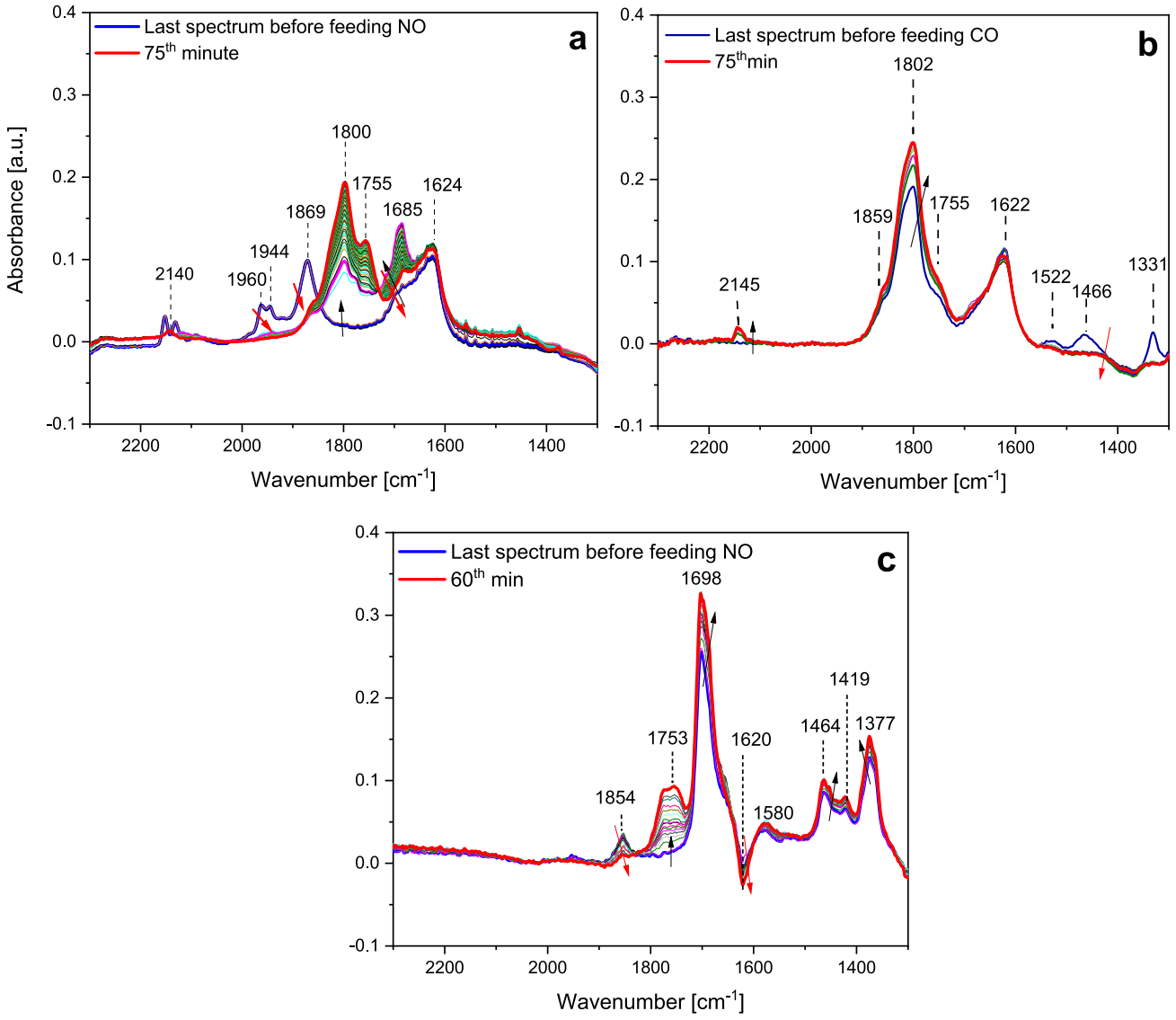

Fig. 5 FT-IR spectra collected at 80 °C during: (**a**) NO adsorption in the presence of CO, (**b**) CO admission in the presence of NO, (**c**) NO admission in the presence of C_3H_6

in the absence of CO (Fig. 1a). Worth to note, when CO is present in the feed stream, neither NO_2 evolution is observed during the TPD part of the run nor low-T NO evolution is seen. As a matter of fact, the low-T NO (and NO_2) evolution in Fig. 1a (CO absence) has been ascribed to nitrate decomposition, which are in fact formed in the absence of CO (see Fig. 2) but not in the presence of CO, as can be seen by inspection of Fig. 4.

Concerning the surface (Fig. 6a), during the initial heating of the catalyst up to 200 °C, a preliminary transformation of the nitrosyls is observed, as in the experiment without CO, from hydrates species to anhydrous moieties (see Fig. 3). This transformation is accompanied by a partial decomposition of the stored nitrosyls, as pointed out by the NO evolution observed in the gas phase below 200 °C. In line with the surface dehydration, the band at 1620 cm^{-1} assigned to adsorbed water decreases upon catalyst heating. These observations are similar to the results reported in the case of NO adsorption and its subsequent TPD, performed in the absence of CO. As the catalyst is further heated up to 300 °C, a rapid decline is observed in the band intensity at around 1810 cm^{-1} and 1856 cm^{-1} related to Pd^{n+} nitrosyls. This decrease is in fact accompanied by a NO evolution which is observed in the gas-phase in the same T-range (see Fig. 1b). Upon further temperature increase, above 300 °C, the complete decomposition of the adsorbed nitrosyls is attained, and no significant NO evolution is seen above this temperature (see Fig. 1b).

The thermal stability of the adsorbed nitrosyls seems to be reduced in the presence of CO, in that a significant decrease of the nitrosyls bands is observed in the 200 °C–300 °C T-range, with a corresponding NO evolution. At variance, in the absence of CO, nitrosyls decomposition was mainly observed at higher temperatures (above 300 °C) (compare Fig. 3 with Fig. 6a). It is speculated that the nitrosyl decomposition is favored by the exothermicity of the CO oxidation reaction as suggested by Castoldi et al. [9] based on the experiments conducted with Pd/FER material under similar operating conditions, as also pointed out by the group of Szanyi et al. [29].

Finally, we note that the amounts of stored NO_x in this case, around 53 $\mu mol/g_{cat}$, is lower than that measured in the absence of CO (near 80 $\mu mol/g_{cat}$), which indicates the fact that CO has a negative impact on NO adsorption. At variance, many studies have shown an increase in NO_x uptake in the presence of CO, see e.g. [5, 14, 30]. In particular, in ref [30]. it is suggested that CO molecules act as additional ligands to provide an alternative pathway with a lower energy barrier in accelerating NO adsorption on hydrated Pd^{2+} ions through the formation of a Pd^{2+}(NO)(CO) complex. The observed decrease in the NO storage capacity observed in this work might be possibly related to the different operating conditions used in this study, possibly in

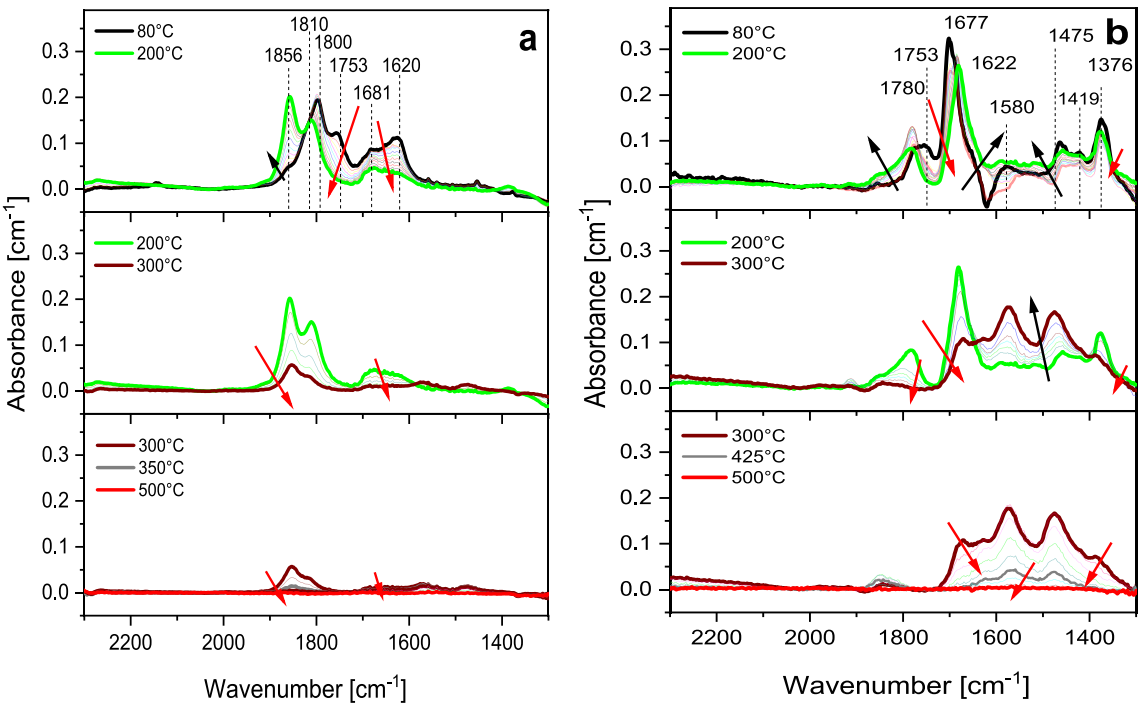

Fig. 6 FT-IR spectra collected during the TPD at 80 °C after NO adsorption in presence of reductants: (**a**) CO and (**b**) C_3H_6. Experimental conditions: TPD in O_2 (3%) + H_2O (2.5%) in He from 80 to 500 °C (10 °C/min)

the sequential feed of CO and then of NO. In particular, the reduction of the Pd sites operated by CO (see Fig. 1b) might decrease the NO storage capacity of the catalyst.

To address this point, an additional experiment has been carried out where NO has been admitted to the catalyst before CO, and results are shown in Fig. 1c (gas phase) and 5b (surface). Note that this run, at variance with the previous experiments with CO, the new experiment has been done in the presence of CO_2 (2%) and with a different CO concentration (800 ppm).

The initial NO uptake upon NO admission to the reactor is very similar to that of Fig. 1a, as expected (the presence of CO_2 is not playing a significant role). Then, upon CO admission to the reactor, when the NO outlet concentration has recovered the inlet concentration level, a negative peak is observed in the NO concentration, indicating a further NO uptake. This is in line with the literature indications previously discussed [5, 14, 30] indicating the beneficial role of CO on NO adsorption. Then, upon NO and CO closure and catalyst heating (TPD, phase 3), the oxidation of CO to CO_2 is observed, along with the desorption of the stored NO desorption. Notably, no NO_2 evolution has been observed, at variance with Fig. 1a.

The results of the surface analysis (Fig. 5b) confirm the increase in the amounts of stored NO upon CO admission, as revealed by the increase of the nitrosyls bands in the region 1700–1900 cm^{-1}. Besides, the formation of a small new band is also observed at 2145 cm^{-1}, associated with the formation of a mixed Pd(CO)(NO) complex as suggested in the literature [30]. Notably, CO admission leads also to the disappearance of the nitrate bands at 1522, 1622 and 1331 cm^{-1}, previously formed upon NO adsorption in the absence of CO. These data hence confirm the promotion of CO in the NO uptake, possibly via the formation of the mixed Pd(CO)(NO) complex previously discussed.

The FT-IR spectra recorded at the end of the storage period (Phase 2), before the TPD run, are very similar to those obtained in the experiment carried out with CO admission before NO (compare the last spectra of Fig. 5a and b), if one neglects the more pronounced shoulder at 1755 cm^{-1} in the spectrum of Fig. 5a. The surface evolution during the final TPD run (not shown) is very similar to what already observed in the case of Fig. 6a.

3.3 NO Adsorption/Desorption in the Presence of C_3H_6

In this section the effect of C_3H_6 presence on NO_x adsorption/desorption has been investigated. Similar to the run carried out with CO, C_3H_6 is adsorbed prior to NO and then NO is admitted to the reactor; eventually the catalyst is heated in the presence of C_3H_6. Note that this run, at variance with previous experiments, has been done in the presence of CO_2 (2%), and hence any CO_2 formation at ppm levels cannot be pointed out.

Upon C_3H_6 admission to the reactor (phase 1 in Fig. 1d), the propylene concentration slowly increases indicating the capability at 80 °C of C_3H_6 to be adsorbed over the catalyst. In fact, at the end of phase 1, the C_3H_6 concentration has not yet reached the inlet concentration value, i.e., 400 ppm.

The FT-IR spectra recorded during the same phase are shown in Fig. 4b. Peaks are observed in the region 1600–1300 cm^{-1}, along with an intense peak at 1701 cm^{-1} and a weak band at around 1854 cm^{-1}. As detailed in the literature [31–34] these peaks are associated to adsorbed propylene. In particular, the peak at 1701 cm^{-1} is characteristic of the C=C vibration mode, while the bands in the range 1470–1370 cm^{-1} are assigned to asymmetric and symmetric $–CH_3$ bending modes, and to $=CH_2$ scissoring. The peak at 1700 cm^{-1} can also be associated to the presence of oxidized species like acetone, acrolein, acetates, giving in fact contributions around 1700 cm^{-1} (C=O stretching) but also in the range 1470–1370 cm^{-1} (COO stretching) [31–35]. A weak band is also formed near 1854 cm^{-1}; the assignment of this band is still under debate but it may be related to some oxidized species originating from propylene. Finally, the negative peak observed at 1618 cm^{-1} is ascribed to bending mode of water, displaced upon propylene adsorption.

Under C_3H_6 flow, NO is admitted to the reactor at 80 °C (phase 2 of Fig. 1d). From the gas-phase profile of NO, NO uptake is observed: this inhibits the C_3H_6 adsorption whose concentration in fact rapidly reaches its inlet concentration value (i.e., 400 ppm). Of note, the concentration of NO reaches steady state level faster than in the presence of CO or with no reductants, indicating a lower amount of adsorbed NO_x in the presence of adsorbed propylene. Calculation showed that the amount of stored NO is in fact near 45 µmol NO_x/g_{cat}. Concerning the surface phase (Fig. 5c), IR features at 1464, 1419 and 1377 cm^{-1} were not much affected by NO admission. However, a new broad band with two maxima is observed in the range 1800–1740 cm^{-1}, which is ascribed to the NO stretching of $Pd^{n+}(NO)(X)$ complexes where X can be C_3H_6, acetone or water [11, 31]. The formation of Pd-NO-olefins complexes have been observed for the first time by Khivantsev et al. [11] upon contacting Pd^{+2} nitrosyls with ethylene, and the formation of a new N–O stretching vibrational feature at 1774 cm^{-1} has been observed. As a matter of facts, in our case the band near 1700 cm^{-1} slightly increase upon NO admission in the presence of propylene whereas the band at 1854 cm^{-1} disappears.

Then, after NO adsorption, the catalyst was heated up to 500 °C under flow of C_3H_6 (phase 3). Gas-phase data are shown in Fig. 1d: two NO desorption peaks are observed, i.e., a minor low-temperature peak with a maximum at 220 °C and a sharp high temperature peak centered at around 430 °C. Upon heating, an initial desorption of propylene and

water is also observed; then the propylene concentration rapidly decreases being oxidized by O_2 with formation of CO_2.

The FT-IR spectra recorded during this phase have been displayed in three different T-ranges in Fig. 6b. In temperature range 80–200 °C, the band observed at 1753 cm^{-1} related to $Pd^{n+}(NO)(X)$ complexes rapidly decreases indicating the decomposition of these NO-containing species. The decrease of the band at 1753 cm^{-1} is accompanied by the increase of the band at 1780 cm^{-1} with a shoulder at about 1850 cm^{-1}, which might be related to the formation of Pd^{+} and Pd^{2+} nitrosyl species, respectively, formed upon readsorption of NO upon decomposition of $Pd^{n+}(NO)(X)$ complexes. In fact, no significant NO desorption is observed during this interconversion as pointed out by the small NO evolution in the gas phase below 200 °C.

In this temperature range a shift of the intense band near 1700 cm^{-1} down to 1677 cm^{-1} is also observed, possibly associated to the formation of oxidized species like acrolein [36], whereas the bands in the range of 1370–1450 cm^{-1} are apparently not much affected.

Upon further temperature increase (200–300 °C), a significant change in the spectra can be observed. In particular, an increase of the band at 1475 and 1580 cm^{-1}, associated to carboxylate and carbonate species is well evident [33, 36] accompanied by a simultaneous decrease of the bands at 1376 and 1419 cm^{-1} associated to adsorbed propylene. This indicates the propylene oxidation, as also pointed out by the concomitant drop of the concentration of C_3H_6 that is observed in the gas phase as the temperature rises above 200 °C (Fig. 1d). The band at 1677 cm^{-1} related to the presence of acrolein also decreases, along with that of the nitrosyls at 1780 and 1854 cm^{-1}. This is in line with the concomitant appearance of the low-temperature NO desorption peak observed in the gas-phase (phase 3 of Fig. 1d) with maximum at 220 °C.

As the catalyst is further heated (300–500 °C), an almost complete desorption of the carbonaceous species (carboxylates, carbonates, etc.) adsorbed on the surface is observed, resulting in the decline of the complex group of bands in the range 1700–1300 cm^{-1} (Fig. 6b). This is also accompanied by an increase in the CO_2 concentration during phase 3 of Fig. 1d. Notably, a sharp NO desorption peak is observed in the gas phase at high temperatures, with maximum near 430 °C. However, no significant nitrosyl decomposition is observed on the surface, being their surface concentration very low already at 300 °C. It is therefore speculated that at high temperatures NO is adsorbed on the catalyst surface not in the form of nitrosyls, but as organic nitro-compound characterized by bands in the region 1700–1300 cm^{-1} [36, 37], i.e., in the region where the bands of the product originating upon propylene oxidation are present. Decomposition of such organic nitro-compound originates the high-T NO peak that is visible in the TPD trace of Fig. 1d.

4 Conclusive Remarks

In this work, mechanistic aspects of NO adsorption/desorption over a home-made 1 wt% Pd/SSZ-13 PNA material were examined through NO_x adsorption and desorption experiments conducted in a micro-reactor and operando FT-IR. The effects on the NO adsorption/desorption characteristics due to the presence of other gaseous species like CO and C_3H_6 has also been investigated.

The experimental findings demonstrate that Pd/SSZ-13 is fairly effective to store NO even under the presence of exhaust species such as propylene and CO. However, the presence of such species significantly affects the NO adsorption characteristics, and the thermal stability of the adsorbed NO_x species as well. In the absence of propylene and CO, operando FT-IR spectroscopy demonstrated the formation of Pd^{n+} nitrosyls upon NO adsorption, particularly involving Pd moieties with oxidation states 1 and 2 and leading to the formation of both anhydrous $Pd^{n+}(NO)$ and $Pd^{n+}(NO)(H_2O)$ complexes upon contacting NO in presence of O_2 and H_2O at 80 °C. Nevertheless, bands relating to monodentate and bidentate nitrates were apparent as well. The NO_x storage capacity of Pd/SSZ-13 evaluated to be near 80 $\mu mol_{NO}/g_{cat}$ at 80 °C in the presence of O_2 and H_2O, corresponding to a NO/Pd molar ratio of 0.8. Nitrates show poor thermal stability in that decompose at low temperatures leading to the evolution of NO and NO_2. At variance, nitrosyls species show higher stability: these species initially dehydrate upon heating and eventually decompose above 300 °C with evolution of NO, related to the decomposition of nitrosyls formed of Pd^{+} and Pd^{2+}.

When CO is contacted with the catalyst, the Pd sites are reduced and carbonyl species over Pd^{2+}, Pd^{+} and Pd^{0} are apparent. Upon NO admission in the presence of CO, NO displaces carbonyls and is readily adsorbed as hydrated/anhydrous nitrosyls on Pd^{n+} at the expenses of carbonyls. However, a slight reduction of the amounts of adsorbed NO (53 vs. 80 $\mu mol_{NO}/g_{cat}$) is observed, possibly due to the reduction of the Pd storage sites. The presence of CO reduces the thermal stability of the adsorbed nitrosyls as well, possibly due to the heat released during CO oxidation: as a matter of facts, nitrosyls decomposition is observed to occur mostly below 300 °C. However when CO is admitted after NO, that prevents the reduction of the Pd sites, a slight increase in the storage capacity is observed, very likely due to the formation of a transient Pd(CO)(NO) complex whose presence accelerates NO adsorption, as suggested in the literature.

The presence of C_3H_6 also affects the NO adsorption/desorption characteristics. Propylene is significantly adsorbed on the catalyst and formation of oxidized species is also apparent, like acetone, acrolein and acetates,

characterized by C=O and COO stretching modes. When NO is adsorbed in the presence of propylene, the NOx uptake is affected by the presence of adsorbed propylene, and in fact only around 45 μmol NO_x/g_{cat} could be stored. In this case, NO is adsorbed in the form of $Pd^{n+}(NO)(X)$ complexes, (X) being C_3H_6, acetone or water. Upon heating, propylene and water desorb, and the $Pd^{n+}(NO)(X)$ complexes decompose. Nitrosyls are also formed due to NO readsorption. These species decompose with a maximum at 220 °C. A high-T NO desorption peak is also observed, likely related to the decomposition of organic nitro-compounds formed as a result of NO adsorption at high temperatures.

Funding Open access funding provided by Politecnico di Milano within the CRUI-CARE Agreement.

References

1. Ryou Y, Lee J, Cho SJ, Lee H, Kim CH, Kim DH (2017) Activation of Pd/SSZ-13 catalyst by hydrothermal aging treatment in passive NO adsorption performance at low temperature for cold start application. Appl Catal B 212:140–149. https://doi.org/10.1016/j.apcatb.2017.04.077
2. Chen HY, Mulla S, Weigert E, Camm K, Ballinger T, Cox J, Blakeman P (2013) Cold start concept (CSC™) a novel catalyst for cold start emission control. SAE Int J Fuels Lubr 6(2):372–381. https://doi.org/10.4271/2013-01-0535
3. Gu Y, Epling WS (2019) Passive NOx adsorber: an overview of catalyst performance and reaction chemistry. Appl Catal A 570:1–14. https://doi.org/10.1016/j.apcata.2018.10.036
4. Kim P, Van der Mynsbrugge J, Aljama H, Lardinois TM, Gounder R, Head-Gordon M, Bell AT (2022) Investigation of the modes of NO adsorption in Pd/H-CHA. Appl Catal B 304:120992. https://doi.org/10.1016/j.apcatb.2021.120992
5. Zheng Y, Kovarik L, Engelhard MH, Wang Y, Wang Y, Gao F, Szanyi J (2017) Low-temperature Pd/zeolite passive NOx adsorbers—structure, performance, and adsorption chemistry. J Phys Chem C 121(29):15793–15803. https://doi.org/10.1021/acs.jpcc.7b04312
6. Lee J, Ryou Y, Cho SJ, Lee H, Kim CH, Kim DH (2018) Investigation of the active sites and optimum Pd/Al of Pd/ZSM-5 passive NO adsorbers for the cold-start application: evidence of isolated-Pd species obtained after a high-temperature thermal treatment. Appl Catal B 226:71–82. https://doi.org/10.1016/j.apcatb.2017.12.031
7. Theis JR, Lambert CK (2015) An assessment of low temperature NOx adsorbers for cold-start NOx control on diesel engines. Catal Today 258:367–377. https://doi.org/10.1016/j.cattod.2015.01.031
8. Zhao H, Hill AJ, Ma L, Bhat A, Jing G, Schwank JW (2021) Progress and future challenges in passive NO adsorption over Pd/zeolite catalysts. Catal Sci Technol. https://doi.org/10.1039/D1CY01084K
9. Castoldi L, Matarrese R, Morandi S, Ticali P, Lietti L (2021) Low-temperature Pd/FER NOx adsorbers: operando FT-IR spectroscopy and performance analysis. Catal Today 360:317–325. https://doi.org/10.1016/j.cattod.2020.02.019
10. Burch SD, Potter TF, Keyser MA, Brady MJ, Michaels KF (1995) Reducing cold-start emissions by catalytic converter thermal management. SAE transactions, Pennsylvania, pp 348–353
11. Khivantsev K, Jaegers NR, Koleva IZ, Aleksandrov HA, Kovarik L, Engelhard M, Gao F, Wang Y, Vayssilov GN, Szanyi J (2019) Stabilization of super electrophilic Pd^{+2} cations in small-pore SSZ-13 zeolite. J Phys Chem C 124(1):309–321. https://doi.org/10.1021/acs.jpcc.9b06760
12. Gupta A, Kang SB, Harold MP (2021) NOx uptake and release on Pd/SSZ-13: impact of feed composition and temperature. Catal Today 360:411–425. https://doi.org/10.1016/j.cattod.2020.01.018
13. Chen HY, Collier JE, Liu D, Mantarosie L, Durán-Martín D, Novák V, Rajaram RR, Thompsett D (2016) Low temperature NO storage of zeolite supported Pd for low temperature diesel engine emission control. Catal Lett https://doi.org/10.1007/s10562-016-1794-6
14. Khivantsev K, Gao F, Kovarik L, Wang Y, Szanyi J (2018) Molecular level understanding of how oxygen and carbon monoxide improve NOx storage in palladium/SSZ-13 passive NOx adsorbers: the role of NO+ and Pd (II)(CO)(NO) species. J Phys Chem C 122(20):10820–10827. https://doi.org/10.1021/acs.jpcc.8b01007
15. Lee J, Ryou Y, Hwang S, Kim Y, Cho SJ, Lee H, Kim CH, Kim DH (2019) Comparative study of the mobility of Pd species in SSZ-13 and ZSM-5, and its implication for their activity as passive NO x adsorbers (PNAs) after hydro-thermal aging. Catal Sci Technol 9(1):163–173. https://doi.org/10.1039/C8CY02088D
16. Porta A, Pellegrinelli T, Castoldi L, Matarrese R, Morandi S, Dzwigaj S, Lietti L (2018) Low temperature NOx adsorption study on Pd-promoted zeolites. Top Catal 61(18):2021–2034. https://doi.org/10.1007/s11244-018-1045-8
17. Khivantsev K, Jaegers NR, Kovarik L, Hanson JC, Tao F, Tang Y, Zhang X, Koleva IZ, Aleksandrov HA, Vayssilov GN, Wang Y (2018) Achieving atomic dispersion of highly loaded transition metals in small-pore zeolite SSZ-13: high-capacity and high-efficiency low-temperature CO and passive NOx adsorbers. Angew Chem Int Ed 57(51):16672–16677. https://doi.org/10.1002/anie.201809343
18. Chakarova K, Ivanova E, Hadjiivanov K, Klissurski D, Knözinger H (2004) Co-ordination chemistry of palladium cations in Pd-H-ZSM-5 as revealed by FTIR spectra of adsorbed and co-adsorbed probe molecules (CO and NO). Phys Chem Chem Phys 6(013):3702–3709. https://doi.org/10.1039/B401934B
19. Hadjiivanov KI (2000) Identification of neutral and charged Nx Oy surface species by IR spectroscopy. Catal Rev 42(1–2):71–144. https://doi.org/10.1081/CR-100100260
20. Lobree LJ, Aylor AW, Reimer JA, Bell AT (1999) NO reduction by CH_4in the presence of O_2over Pd-H-ZSM-5. J Catal 181(2):189–204. https://doi.org/10.1006/jcat.1998.2303
21. Descorme C, Gélin P, Primet M, Lécuyer C (1996) Infrared study of nitrogen monoxide adsorption on palladium ion-exchanged

ZSM-5 catalysts. Catal Lett 41(3):133–138. https://doi.org/10.1007/BF00811479
22. Song I, Khivantsev K, Wu Y, Bowden M, Wang Y, Szanyi J (2022) Unusual water-assisted NO adsorption over Pd/FER calcined at high temperatures: the effect of cation migration. Appl Catal B 318:121810. https://doi.org/10.1016/j.apcatb.2022.121810
23. Mandal K, Gu Y, Westendorff KS, Li S, Pihl JA, Grabow LC, Epling WS, Paolucci C (2020) Condition-dependent Pd speciation and NO adsorption in Pd/zeolites. ACS Catal 10(21):12801–12818. https://doi.org/10.1021/acscatal.0c03585
24. Kunal P, Toops TJ, Kidder MK, Lance MJ (2021) Deactivation trends of Pd/SSZ-13 under the simultaneous presence of NO, CO, hydrocarbons and water for passive NOx adsorption. Appl Catal B 299:120591. https://doi.org/10.1016/j.apcatb.2021.120591
25. Hadjiivanov KI, Vayssilov GN (2002) Characterization of oxide surfaces and zeolites by carbon monoxide as an IR probe molecule. Elsevier, Amsterdam, pp 307–511
26. Aylor AW, Lobree LJ, Reimer JA, Bell AT (1997) Investigations of the dispersion of Pd in H-ZSM-5. J Catal 172(2):453–462. https://doi.org/10.1006/jcat.1997.1893
27. Groppo E, Bertarione S, Rotunno F, Agostini G, Scarano D, Pellegrini R, Leofanti G, Zecchina A, Lamberti C (2007) Role of the support in determining the vibrational properties of carbonyls formed on Pd supported on SiO_2−Al_2O_3, Al_2O_3, and MgO. J Phys Chem C 111(19):7021–7028. https://doi.org/10.1021/jp0666434
28. Spezzati G, Su Y, Hofmann JP, Benavidez AD, DeLaRiva AT, McCabe J, Datye AK, Hensen EJ (2007) Atomically dispersed Pd–O species on CeO_2 (111) as highly active sites for low-temperature CO oxidation. ACS Catal 7(10):6887–6891. https://doi.org/10.1021/jp0666434
29. Khivantsev K, Wei X, Kovarik L, Jaegers NR, Walter ED, Tran P, Wang Y, Szanyi J (2022) Palladium/ferrierite versus palladium/SSZ-13 passive NOx adsorbers: adsorbate-controlled location of atomically dispersed palladium (II) in ferrierite determines high activity and stability. Angew Chem Int Ed 61(3):e202107554. https://doi.org/10.26434/chemrxiv.12385577
30. Song I, Khivantsev K, Wang Y, Szanyi J (2022) Elucidating the role of CO in the NO storage mechanism on Pd/SSZ-13 with in situ DRIFTS. J Phys Chem C 126(3):1439–1449. https://doi.org/10.1021/acs.jpcc.1c10163
31. Liu C, Wang J, Chen Z, Wang J, Shen M (2021) Improvement of NOx uptake/release over Pd/beta by propylene: shielding effect of intermediates on adsorbed NOx species. Phys Chem Chem Phys 23(9):5261–5269. https://doi.org/10.1039/D0CP06075E
32. Panov A, Fripiat JJ (1998) An infrared spectroscopic study of acetone and mesityl oxide adsorption on acid catalyst. Langmuir 14(14):3788–3796. https://doi.org/10.1021/la971359c
33. Sobczak I, Kusior A, Ziolek M (2008) FTIR study of NO, C_3H_6 and O_2 adsorption and interaction on gold modified MCM-41 materials. Catal Today 137(2–4):203–208. https://doi.org/10.1016/j.cattod.2007.11.061
34. Benaliouche F, Boucheffa Y, Thibault-Starzyk F (2012) In situ FTIR studies of propene adsorption over Ag-and Cu-exchanged Y zeolites. Microporous Mesoporous Mater 147(1):10–16. https://doi.org/10.1016/j.micromeso.2011.04.040
35. Čapek L, Novoveska K, Sobalik Z, Wichterlová B, Cider L, Jobson E (2005) Cu-ZSM-5 zeolite highly active in reduction of NO with decane under water vapor presence: comparison of decane, propane and propene by in situ FTIR. Appl Catal B 60(3–4):201–210. https://doi.org/10.1016/j.apcatb.2005.02.033
36. Mosqueda-Jiménez BI, Jentys A, Seshan K, Lercher JA (2003) On the surface reactions during NO reduction with propene and propane on Ni-exchanged mordenite. Appl Catal B 46(1):189–202. https://doi.org/10.1016/S0926-3373(03)00212-1
37. Dorado F, De Lucas A, García PB, Valverde JL, Romero A (2006) Preparation of Cu-ion-exchanged Fe-PILCs for the SCR of NO by propene. Appl Catal B 65(3–4):175–184. https://doi.org/10.1016/j.apcatb.2006.01.008